The Cryosphere Discuss., https://doi.org/10.5194/tc-2018-190
Manuscript under review for journal The Cryosphere
Discussion started: 18 September 2018


# Brief Communication: Evaluation and comparisons of permafrost map over Qinghai-Tibet Plateau based on inventory of in-situ evidence

Bin Cao[1], Tingjun Zhang[1], Qingbai Wu[2], Yu Sheng[2], Lin Zhao[3], and Defu Zou[3]

[1]Key Laboratory of Western China's Environmental Systems (Ministry of Education), College of Earth and Environmental Sciences, Lanzhou University, Lanzhou, China
[2]State Key Laboratory of Frozen Soil Engineering, Cold and Arid Regions Environmental and Engineering Research Institute, Chinese Academy of Sciences, Lanzhou, China
[3]Cryosphere Research Station on the Qinghai-Tibet Plateau, State Key Laboratory of Cryospheric Science, Cold and Arid Regions Environmental and Engineering Research Institute, Chinese Academy of Sciences, Lanzhou, China

**Correspondence:** Tingjun Zhang (tjzhang@lzu.edu.cn)

**Abstract.** Many maps have been produced to estimate permafrost distribution over the Qinghai-Tibet Plateau, however, the evaluation and comparisons of them are poorly understood due to limited evidence. Using a large number data from various sources, we present the inventory of permafrost presence/absence with 1475 sites/plots over the QTP. Based on the in-situ measurements, our evaluation results showed a wide range of map performance with the overall accuracy of about 59–82%, and the estimated permafrost region (1.42–1.84$\times 10^6$ km$^2$) and area (0.76–1.25$\times 10^6$ km$^2$) are extremely large. The low agreement in areas near permafrost boundary and fragile landscapes require improved method considering more controlling factors at both medium-large and local scales.

## 1 Introduction

Permafrost is one of the major components of the cryosphere due to its large spatial extent. The Qinghai-Tibet Plateau (QTP), known as the Third Pole, has the largest extent of permafrost in the low-middle latitudes. Permafrost over the QTP was reported to be sensitive to global warming mainly due to high temperature (< -2 °C) (Wu and Zhang, 2008), and its distribution has strong influences on hydrological processes (e.g., Cheng and Jin (2013)), biogeochemical processes (e.g., Mu et al. (2017)), and human systems (e.g., Wu et al. (2016)).

Many maps have been produced to estimate permafrost distribution and ground ice conditions at different scales over the QTP (Ran et al., 2012). Typically, frozen ground is classified into permafrost and seasonally frozen ground, and information on the extent, i.e. the areal abundance, of permafrost is available for some of the maps (Ran et al., 2012). These maps significantly improved the understanding of permafrost distribution over the QTP, however, limited in-situ measurements and the different classification systems and compilation approaches used make the comparison of maps a challenge. With the availability of high-resolution spatial data sets (e.g., surface air temperature and land surface temperature), several empirical and (semi-)physical models are now applied in permafrost distribution simulations at fine scales (Nan et al., 2013; Zhao et al., 2017; Zou et al., 2017; Wu et al., 2018). Additionally, the QTP was involved in hemisphere or global maps, e.g., the Circum-Arctic Map of Permafrost and Ground-ice Conditions leaded by the International Permafrost Association (referenced as IPA map) (Brown, 1997), and the global permafrost zonation (referenced as $PZI_{global}$) map derived by Gruber (2012).

Despite the increasing efforts made on permafrost mapping, existing maps over the QTP so far have not been evaluated with large enough data sets. This would weaken their applications in permafrost and related studies, e.g., as a boundary condition for eco-hydrological model simulations. The global warming and increasing amount of infrastructure built on permafrost add both environmental and engineering relevance to investigating permafrost distribution, and makes studies of evaluating and comparing existing permafrost maps of great importance.

A large amount of permafrost presence/absence evidence has been collected using a wide variety of methods (e.g., ground temperature, soil pits, and geophysics) on the QTP since 2000. In this study, we aim

1. to provide the first inventory of permafrost presence/absence evidence for the QTP;

2. to evaluate and compare existing permafrost maps on the QTP, using the new inventory data.

## 2 Data and methods

### 2.1 Inventory of permafrost presence/absence evidence

Four methods, including borehole temperature (BH), soil pit (SP), ground surface temperature (GST), and ground-penetrating radar (GPR), were used to acquire evidence of permafrost presence or absence (Figure 1). BH and SP provide direct evidence of permafrost presence or absence based on mean annual ground temperature (MAGT) and/or ground ice observations, and hence have high certainty (Cremonese et al., 2011). GST, referred as soil temperature at the depth of 0.05 or 0.1 m here, was used to establish permafrost presence/absence for specific sites due to the MAGT could be derived as the difference of thermal offset and mean annual ground surface temperature (MAGST) (Hasler et al., 2015). While thermal offset is spatially variable depending on soil and temperature conditions, it is relatively small on the QTP compared with northern high latitudes environments due to prevalent coarse soil and low soil moisture content. The maximum thermal offset under natural conditions reported for the QTP is 0.79 °C (referenced as maximum thermal offset, $TO_{max}$) (Wu et al., 2002, 2010; Lin et al., 2015). In this study, sites with $MAGST + TO_{max} \leqslant 0$ °C are considered as permafrost sites and the confidence in this is classified based on MAGST and the length of the observation period:

- MAGST $\leqslant$ -2 °C & observations $\geqslant$ 3 years: medium certainty;
- MAGST $>$ -2 °C & $MAGST + TO_{max} \leqslant 0$ °C: low certainty;
- MAGST $<$ 0 °C & $MAGST + TO_{max} > 0$ °C: ambiguous, point removed from evidence collection;
- MAGST $>$ 0 °C : medium certainty of permafrost absence.

The suitability of GPR for detecting permafrost derives from the dielectric contrast between liquid water and ice (Moorman et al., 2003), and it may face the challenge of distinguishing presence of permafrost in areas with low soil moisture content (Cao et al., 2017b). Here, GPR data are considered as indicating the presence of permafrost (medium certainty) only if a clear permafrost reflection could be established in a published study.

### 2.2 Existing maps over the QTP

Table 1 gives the summary of most widely used and recent developed permafrost maps over the QTP. In general, permafrost maps over the QTP could be classified as (1) binary, using categorical classification with permafrost presence [1] or absence [0], and (2) continuous, using continuous probability or indices [0–1] to represent proportion of an area that is underlain by permafrost. The IPA map, which is may the most widely used binary map, was complied by assembling all readily available data on the characteristics and distribution of permafrost (Ran et al., 2012). The most recent efforts were made by Zou et al. (2017) using the temperature at the top of permafrost (TTOP) model (referenced as $QTP_{TTOP}$ map) forced by land surface temperature (or freezing and thawing indices) considering soil properties, and by Wu et al. (2018) based on Noah land surface model (referenced as $QTP_{Noah}$ map) as well as gridded meteorological dataset (e.g., surface air temperature, radiation, and precipitation). Though, these two binary maps are expected to be superior by using the latest measurements and advanced methods, they were evaluated using limited and narrow distributed data (∼200 sites for the $QTP_{TTOP}$ map and 56 sites for the $QTP_{Noah}$ map). On the other hand, the $PZI_{global}$ map, which gives continuous index for permafrost distribution, is derived through its heuristic-empirical relationship with mean annual air temperature (MAAT) based on generalized linear models (Gruber, 2012). The model parameters are established largely based on the boundaries of continuous and isolated permafrost in the IPA map and do not use field observations. Additionally, two cases, including cold (conservative or more permafrost) and warm (anti-conservative or less permafrost), were introduced into the map to allow the propagation of uncertainty caused by input dataset and model suitability. A part of the QTP of the $PZI_{global}$ was evaluated using rock glaciers, considered as indicators of permafrost conditions, based on remote sensing imagery (Schmid et al., 2015). Rock glaciers, however are of absence in much of the QTP due to very low precipitation (Gruber et al., 2017).

### 2.3 Climate variables and topography

The slope and aspect of the inventory were derived from a DEM with 3 arcsec, which is aggregated from the Global Digital Elevation Model version 2 (GDEM2) by averaging to avoid the noise in the original dataset (Cao et al., 2017a). The thermal state of permafrost and its spatial distribution result from the long-term interaction of climate and subsurface. Additionally, vegetation and snow coverage play important roles in permafrost distribution through influencing the energy exchange between the atmosphere and the ground surface (Norman et al., 1995; Zhang, 2005). In this study, three climate variables of MAAT, mean annual snow cover days (MASCD), and the annual maximum normalized difference vegetation index (NDVI) were hence selected here to test the representative of the inventory for permafrost map evaluation. The MAAT with resolution of 1 km is from Gruber (2012) representing the referenced period 1961–1990. The MASCD (about 500 m) was derived from daily snow cover product developed by Wang et al. (2015) based on MODIS products (MOD10A1 and MYD10A1). To improve the comparison of MASCD, it is scaled to 0–1 through dividing the total days of a given year, and the mean MASCD during 2003–2010 was produced as a predictor. The annual maximum NDVI is from MODIS/Terra Vegetation Indices 16-day product (MOD13Q1, v006) with a resolution of 250 m. The annual maximum NDVI ($NDVI_{max}$) was computed for each year during 2001–2017 to approximately represent the amount of vegetation, and then aggregated as a median for the entire period to avoid sensitivity to extreme values. The outline of QTP is from Zhang et al. (2002), glacier outlines is from Liu et al. (2015) representing conditions in 2010, and lake data is provided by the Third Pole Environment Database.

### 2.4 Statistics and evaluation of permafrost distribution maps

In this study, it is important to understand the difference between extent of permafrost region and permafrost area. Permafrost region is the area permafrost likely present, however, the permafrost may not be everywhere. Permafrost area is where actually underlain by permafrost (Zhang et al., 2000). To estimate permafrost region and area based on the PZI as model output, specified thresholds are required for both the extent of permafrost region and permafrost area. By following Gruber (2012), only the areas with PZI $\geq 0.01$ were selected for further analysis, permafrost region is defined as the area with PZI $\geq 0.1$, and permafrost area was derived as PZI multiplied pixel area.

Evaluations of the maps with categorical types are conducted using classification accuracies (Wang et al., 2015):

$$PCC_{PF} = \frac{PF_T}{PF_T + PF_F} \times 100\% \tag{1}$$

$$PCC_{NPF} = \frac{NPF_T}{NPF_T + NPF_F} \times 100\% \tag{2}$$

$$PCC_{tol} = \frac{PF_T + NPF_T}{PF_T + PF_F + NPF_T + NPF_F} \times 100\% \tag{3}$$

where subscripts of $T$ (True, correctly classified) and $F$ (False, incorrectly classified) identify corrections of classification. In this case, $PF_T$ is permafrost presence sites/plots correctly classified as permafrost, while $PF_F$ is incorrectly classified as non-permafrost. $NPF_T$ is permafrost absence sites correctly classified as non-permafrost, and $NPF_F$ is incorrectly classified as permafrost. $PCC$ is Percent of sites/plots Correctly Classified, and the subscripts of $PF$, $NPF$, and $tol$ means permafrost, non-permafrost, and total sites/plots, respectively. For the PZI map, the PZI of 0.5 was used as the threshold of permafrost presence and absence (Boeckli et al., 2012; Azócar et al., 2017), and the above index were tested. To avoid the impact of uneven distribution of sample numbers for permafrost presence and absence, the Cohen's kappa coefficient ($\kappa$), which measures inter-rater agreement for categorical items (Landis and Koch, 1977), was introduced here for map evaluation.

## 3 Results and discussion

### 3.1 Evidence of Permafrost Presence or Absence

Based on the classification algorithm of permafrost presence/absence, there are in total 1475 sites/plots contained in the inventory (Figure 1). Among the 1475 evidences, there are 1141 (77.4%) sites measured by BH, 176 (11.9%) sites by GST, 156 (10.6%) plots by GPR, and 30 (2.0%) sites by SP (Figure 1c). There are 1012 (68.6%) permafrost presence sites/plots and 463 (31.4%) permafrost absence sites/plots. Where original field evidence of permafrost presence/absence is located within the same grid cell (30 arcsec, ~1 km), they were aggregated based on their major value. For grid with one permafrost site and one non-permafrost site, the nearer site from the grid center was used to represent the grid. As a result, there are in total 1040 aggregated points/plots left for permafrost maps evaluation. These aggregated evidences extend over a large area of the QTP (latitude: 27.73–38.95°N, longitude: 75.06–103.57°E) (Figure 1d). The evidence cover a wide elevation range from about 1600 m to over 5200 m, however, the majority (91.4%) is located between 3500 m and 5000 m. While the inventory showed an even distribution of aspects with 27.3% on the east slope, 27.9% on the south slope, 22.0% on the west slope, and 22.6% on the north slope, most of the evidence (96.2%) have slope angles less than 20° (Figure 1c).

Figure 1d, e and f present the coverage of aggregated evidence for selected climate variables, which could significantly influence permafrost distribution, comparing to the entire QTP. The 1040 aggregated field sites/plots showed a relatively narrower MAAT range (-10.5–15.7 °C with Q25 lower quantile = -5.9 °C and Q75 upper quantile = -3.4 °C) comparing to the entire QTP with MAAT between -25.6 and 22.1 °C (Q25 lower quantile = -6.6 °C and Q75 upper quantile = -0.41 °C), and only 1.3% sites/plots located in the area with MAAT $<$ -8 °C. However, the evidence (84.9%) was mainly occurred in the most sensitive band (from -8 to -2 °C) of permafrost presence/absence changing with MAAT (Gruber, 2012; Cao et al.). There is a slight bias for scaled MASCD coverage with little measurements (7.6%) in high scaled MASCD ($>$ 0.20) area due to the harsh climate and inconvenient access. The annual maximum NDVI at evidence sites/plots has a wide coverage for the QTP with the range of 0.05–0.88. The higher mean NDVI for evidence (0.45 at the sample sites/plots and 0.37 for the QTP) is due to the measurements are occurred in flat areas with relatively dense vegetation cover. The exploration of inventory indicated the evaluation presented in this study to be representative for most of the QTP, and may have pronounced uncertainty in steep and regular snow covered regions.

### 3.2 Evaluation and comparison of existing maps

The new inventory was used to evaluate existing permafrost maps derived with different methods (Table 1). In general, these permafrost maps showed different performances, including fair agreement for the $\text{PZI}_{\text{warm}}$ (the subscript for PZI map refers different cases and assumptions for PZI model parameters) and IPA maps, moderate agreement for the $\text{QTP}_{\text{Noah}}$, $\text{PZI}_{\text{norm}}$, and $\text{PZI}_{\text{cold}}$ maps, and substantial agreement for the $\text{QTP}_{\text{TTOP}}$ maps, with a wide spread of $\kappa$ from 0.24 to 0.60. Additionally, the range of estimated permafrost region (1.42–1.84 $\times$ $10^6$ km$^2$, or 30% difference) and area (0.76–1.25 $\times$ $10^6$ km$^2$, or 64.4% difference) are extremely large.

$\text{QTP}_{\text{TTOP}}$ map achieved the best performance for permafrost distribution over the QTP with the highest $\kappa$ (0.60, substantial agreement) and $PCC_{tol}$ (82.0%). The $\text{PZI}_{\text{norm}}$ and $\text{PZI}_{\text{cold}}$ maps, judged as moderate agreement ($\kappa$ = 0.57) with in-situ measurements, showed slightly worse performance comparing with the $\text{PZI}_{\text{TTOP}}$ map. While the IPA and $\text{QTP}_{\text{Noah}}$ maps performed slightly better (1.8–3.1% higher) for permafrost areas than the $\text{QTP}_{\text{TTOP}}$ and $\text{PZI}_{\text{cold}}$ maps, they suffer considerable underestimation of non-permafrost area (14.1–39.8% lower for $PCC_{NPF}$). Though the $\text{QTP}_{\text{Noah}}$ map was derived using coupled land surface model (Noah), the relatively worse performance, especially for non-permafrost area ($PCC_{\text{NPF}}$ = 49.5%), is likely caused by inputing coarse-scale forcing dataset (0.1° resolution or ∼10 km) (Chen et al., 2011) and by the uncertainty of soil texture dataset (Yang et al., 2010). Great difference of permafrost region ($0.42 \times 10^6$ km$^2$, or 25% of the normal case) and area ($0.49 \times 10^6$ km$^2$, or 49% of the normal case) was found for the three cases of $PZI_{global}$ map though the upper and lower bounds of MAAT are only changed about 5%. It is not surprising that the IPA map has fair agreement ($\kappa$ = 0.24) as less observations were compiled and the method used are more suitable for high latitudes (Ran et al., 2012). The worst performance of $PZI_{warm}$ map (or good performance of $PZI_{cold}$ map) indicated permafrost is more prevalent than most of the other regions even when the climate conditions, especially the MAAT, are similar. This is very likely because the high soil thermal conductivity due to coarse soil conditions and the cooling effects of minimal snow (Zhang, 2005).

Spatially, the southeastern QTP of non-permafrost areas are better represented in all maps, while misclassification is prevalent in areas near the permafrost boundary and fragile landscapes such as the sources of Yellow River (Figure 2). This is because the permafrost distribution in these areas is not only controlled by medium-large scale climate condition (e.g., MAAT) which is described by the models used, but also strongly influenced by various local factors such as peat layer, thermokarst, soil moisture, and hydrological processes. Specially, about 30.3 (18.5–63.8)% for permafrost presence and about 39.2 (24.7–65.1)% for absence of the misclassification sites in the maps occurred in the MAAT band from -3 to -4 °C, which is expected as the threshold of permafrost presence for most areas. The IPA and $PZI_{warm}$ maps showed a fit that is good only in some areas (e.g., southeastern for the $PZI_{warm}$ map and relatively colder areas for the IPA map) based on the in-situ measurements, and may not represent the permafrost distribution patterns well for the other areas beyond the measurement.

## 4 Conclusions

We compiled an inventory of permafrost presence or absence evidence with 1475 field sites/plots obtained based on diverse methods over the QTP. With wide coverage of topography (e.g., elevation and slope aspect) and climate conditions (e.g., surface air temperature and snow cover), the inventory gives a representative baseline for site-specific permafrost occurrence. The existing permafrost maps over the QTP were better evaluated and compared with the inventory of ground-based evidence, and they showed a wide range of performance with the overall classification accuracy of about 59–82%. The $QTP_{TTOP}$ and $PZI_{cold}$ maps are recommended for representing permafrost distribution over the QTP based on our evaluations. The inadequate sampling is expected to result in uncertainty for map evaluation in steeps and regular snow covered areas, and requires further investigation using systematic samples.

*Data availability.* Inventory of permafrost presence/absence is partly available as supplement, the other evidence not listed is available from the authors upon request.

*Author contributions.* Bin Cao carried out this study by organizing permafrost presence/absence evidence, analyzing data, performing the simulations and by structuring as well as writing the paper. Tingjun Zhang guided the research. Qingbai Wu, Yu Sheng, Lin Zhao, and Defu Zou contributed to organize the permafrost presence/absence dataset.

*Competing interests.* The authors declare that no competing interests are present.

*Acknowledgements.* The authors would like to thank Stephan Gruber and Kang Wang for their constructive suggestions. We thank Zhuotong Nan and Xiaobo Wu for providing the $QTP_{Noah}$ map. This study was supported by the National Natural Science Foundation of China (91325202), the National Key Scientific Research Program of China (2013CBA01802), partly by the Fundamental Research Funds for the Central Universities (lzujbky_2016_281, 862863). We thank CMA (http://cdc.cma.gov.cn/) for providing the surface air and ground surface temperatures, the ASTER dataset is downloaded from United States Geological Survey (http://gdex.cr.usgs.gov/gdex/), glacier inventory is provided by the Environmental and Ecological Science Data Center for West China (http://westdc.westgis.ac.cn/), and lake inventory is from the Third Pole Environment Database (http://www.tpedatabase.cn).

## References


Azócar, G. F., Brenning, A., and Bodin, X.: Permafrost distribution modelling in the semi-arid Chilean Andes, The Cryosphere, 11, 877–890, https://doi.org/10.5194/tc-11-877-2017, 2017.

Boeckli, L., Brenning, A., Gruber, S., and Noetzli, J.: Permafrost distribution in the European Alps: calculation and evaluation of an index map and summary statistics, The Cryosphere, 6, 807–820, https://doi.org/10.5194/tc-6-807-2012, 2012.

Brown, J., F. J. O. H. J. M. E.: Circum-Arctic Map of Permafrost and Ground-ice Conditions, 1997.

Cao, B., Zhang, T., Peng, X., Mu, C., Wang, Q., Zheng, L., Wang, K., and Zhong, X.: Thermal Characteristics and Recent Changes of Permafrost in the Upper Reaches of the Heihe River Basin, Western China, Journal of Geophysical Research: Atmospheres, 0, https://doi.org/10.1029/2018JD028442, https://agupubs.onlinelibrary.wiley.com/doi/abs/10.1029/2018JD028442.

Cao, B., Gruber, S., and Zhang, T.: REDCAPP (v1.0): parameterizing valley inversions in air temperature data downscaled from reanalyses, Geoscientific Model Development, 10, 2905–2923, https://doi.org/10.5194/gmd-10-2905-2017, 2017a.

Cao, B., Gruber, S., Zhang, T., Li, L., Peng, X., Wang, K., Zheng, L., Shao, W., and Guo, H.: Spatial variability of active layer thickness detected by ground-penetrating radar in the Qilian Mountains, Western China, Journal of Geophysical Research: Earth Surface, 122, 574–591, https://doi.org/10.1002/2016JF004018, 2016JF004018, 2017b.

Chen, Y., Yang, K., He, J., Qin, J., Shi, J., Du, J., and He, Q.: Improving land surface temperature modeling for dry land of China, Journal of Geophysical Research: Atmospheres, 116, https://doi.org/10.1029/2011JD015921, d20104, 2011.

Cheng, G. and Jin, H.: Permafrost and groundwater on the Qinghai-Tibet Plateau and in northeast China, Hydrogeology Journal, 21, 5–23, https://doi.org/10.1007/s10040-012-0927-2, https://doi.org/10.1007/s10040-012-0927-2, 2013.

Cremonese, E., Gruber, S., Phillips, M., Pogliotti, P., Boeckli, L., Noetzli, J., Suter, C., Bodin, X., Crepaz, A., Kellerer-Pirklbauer, A., Lang, K., Letey, S., Mair, V., Morra di Cella, U., Ravanel, L., Scapozza, C., Seppi, R., and Zischg, A.: Brief Communication: "An inventory of permafrost evidence for the European Alps", The Cryosphere, 5, 651–657, https://doi.org/10.5194/tc-5-651-2011, 2011.

Gruber, S.: Derivation and analysis of a high-resolution estimate of global permafrost zonation, The Cryosphere, 6, 221–233, https://doi.org/10.5194/tc-6-221-2012, 2012.

Gruber, S., Fleiner, R., Guegan, E., Panday, P., Schmid, M.-O., Stumm, D., Wester, P., Zhang, Y., and Zhao, L.: Review article: Inferring permafrost and permafrost thaw in the mountains of the Hindu Kush Himalaya region, The Cryosphere, 11, 81–99, https://doi.org/10.5194/tc-11-81-2017, 2017.

Hasler, A., Geertsema, M., Foord, V., Gruber, S., and Noetzli, J.: The influence of surface characteristics, topography and continentality on mountain permafrost in British Columbia, The Cryosphere, 9, 1025–1038, https://doi.org/10.5194/tc-9-1025-2015, 2015.

Landis, J. R. and Koch, G. G.: The Measurement of Observer Agreement for Categorical Data, Biometrics, 33, 159–174, http://www.jstor.org/stable/2529310, 1977.

Lin, Z., Burn, C. R., Niu, F., Luo, J., Liu, M., and Yin, G.: The Thermal Regime, including a Reversed Thermal Offset, of Arid Permafrost Sites with Variations in Vegetation Cover Density, Wudaoliang Basin, Qinghai-Tibet Plateau, Permafrost and Periglacial Processes, 26, 142–159, https://doi.org/10.1002/ppp.1840, 2015.

Liu, S., Yao, X., Guo, W., Xu, J., Shangguan, D., Wei, J., Bao, W., and Wu, L.: The contemporary glaciers in China based on the Second Chinese Glacier Inventory (in Chinese with English abstract), Acta Geographica Sinica, 70, 3, https://doi.org/10.11821/dlxb201501001, 2015.

Moorman, B. J., Robinson, S. D., and Burgess, M. M.: Imaging periglacial conditions with ground-penetrating radar, Permafrost and Periglacial Processes, 14, 319–329, https://doi.org/10.1002/ppp.463, 2003.

Mu, C., Zhang, T., Zhao, Q., Su, H., Wang, S., Cao, B., Peng, X., Wu, Q., and Wu, X.: Permafrost affects carbon exchange and its response to experimental warming on the northern Qinghai-Tibetan Plateau, Agricultural and Forest Meteorology, 247, 252 – 259, https://doi.org/https://doi.org/10.1016/j.agrformet.2017.08.009, 2017.

Nan, Z., Huang, P., and Zhao, L.: Permafrost distribution modeling and depth estimation in the Western Qinghai-Tibet Plateau (in Chinese with English abstract), Acta Geographica Sinica, 68, 318, https://doi.org/10.11821/xb201303003, 2013.

Norman, J., Kustas, W., and Humes, K.: Source approach for estimating soil and vegetation energy fluxes in observations of directional radiometric surface temperature, Agricultural and Forest Meteorology, 77, 263 – 293, thermal Remote Sensing of the Energy and Water Balance over Vegetation, 1995.

Ran, Y., Li, X., Cheng, G., Zhang, T., Wu, Q., Jin, H., and Jin, R.: Distribution of Permafrost in China: An Overview of Existing Permafrost Maps, Permafrost and Periglacial Processes, 23, 322–333, https://doi.org/10.1002/ppp.1756, 2012.

Schmid, M.-O., Baral, P., Gruber, S., Shahi, S., Shrestha, T., Stumm, D., and Wester, P.: Assessment of permafrost distribution maps in the Hindu Kush Himalayan region using rock glaciers mapped in Google Earth, The Cryosphere, 9, 2089–2099, https://doi.org/10.5194/tc-9-2089-2015, https://www.the-cryosphere.net/9/2089/2015/, 2015.

Wang, W., Huang, X., Deng, J., Xie, H., and Liang, T.: Spatio-Temporal Change of Snow Cover and Its Response to Climate over the Tibetan Plateau Based on an Improved Daily Cloud-Free Snow Cover Product, Remote Sensing, 7, 169–194, https://doi.org/10.3390/rs70100169, 2015.

Wu, J., Sheng, Y., Wu, Q., and Wen, Z.: Processes and modes of permafrost degradation on the Qinghai-Tibet Plateau, Science in China Series D: Earth Sciences, 53, 150–158, https://doi.org/10.1007/s11430-009-0198-5, 2010.

Wu, Q. and Zhang, T.: Recent permafrost warming on the Qinghai-Tibetan Plateau, Journal of Geophysical Research: Atmospheres, 113, n/a–n/a, https://doi.org/10.1029/2007JD009539, d13108, 2008.

Wu, Q., Yuanlin, Z., and Yongzhi, L.: Application of the Permafrost Table Temperature and Thermal Offset Forecast Model in the Tibetan Plateau, Journal of Glaciology and Geocryology, pp. 24–27, 2002.

Wu, Q., Zhang, Z., Gao, S., and Ma, W.: Thermal impacts of engineering activities and vegetation layer on permafrost in different alpine ecosystems of the Qinghai–Tibet Plateau, China, The Cryosphere, 10, 1695–1706, https://doi.org/10.5194/tc-10-1695-2016, 2016.

Wu, X., Nan, Z., Zhao, S., Zhao, L., and Cheng, G.: Spatial modeling of permafrost distribution and properties on the Qinghai–Tibet Plateau, Permafrost and Periglacial Processes, 29, 86–99, https://doi.org/10.1002/ppp.1971, 2018.

Yang, K., He, J., Tang, W., Qin, J., and Cheng, C. C.: On downward shortwave and longwave radiations over high altitude regions: Observation and modeling in the Tibetan Plateau, Agricultural and Forest Meteorology, 150, 38 – 46, https://doi.org/https://doi.org/10.1016/j.agrformet.2009.08.004, 2010.

Zhang, T.: Influence of the seasonal snow cover on the ground thermal regime: An overview, Reviews of Geophysics, 43, https://doi.org/10.1029/2004RG000157, 2005.

Zhang, T., Heginbottom, J. A., Barry, R. G., and Brown, J.: Further statistics on the distribution of permafrost and ground ice in the Northern Hemisphere, Polar Geography, 24, 126–131, https://doi.org/10.1080/10889370009377692, 2000.

Zhang, Y., Li, B., and Zheng, D.: A discussion on the boundary and area of the Tibetan Plateau in China, Geographical Research, 21, 1, https://doi.org/10.11821/yj2002010001, 2002.

Zhao, S., Nan, Z., Huang, Y., and Zhao, L.: The Application and Evaluation of Simple Permafrost Distribution Models on the Qinghai—Tibet Plateau, Permafrost and Periglacial Processes, 28, 391–404, https://doi.org/10.1002/ppp.1939, 2017.

Zou, D., Zhao, L., Sheng, Y., Chen, J., Hu, G., Wu, T., Wu, J., Xie, C., Wu, X., Pang, Q., Wang, W., Du, E., Li, W., Liu, G., Li, J., Qin, Y., Qiao, Y., Wang, Z., Shi, J., and Cheng, G.: A new map of permafrost distribution on the Tibetan Plateau, The Cryosphere, 11, 2527–2542, https://doi.org/10.5194/tc-11-2527-2017, 2017.

**Table 1.** Summary and evaluation of existing permafrost maps over the Qinghai-Tibet Plateau

| Name | IPA | $QTP_{TTOP}$ | $QTP_{Noah}$ | $PZI_{norm}$ | $PZI_{warm}$ | $PZI_{cold}$ |
|---|---|---|---|---|---|---|
| Year | 1997 | 2017 | 2018 | 2012 | 2012 | 2012 |
| Method | – | semi-physical model | physical model | heuristic GLM | heuristic GLM | heuristic GLM |
| Classification Criteria | categorical | categorical | categorical | continuous | continuous | continuous |
| Scale | 1:10,000,000 | ~1 km | 0.1° (~10 km) | ~1 km | ~1 km | ~1 km |
| $PCC_{PF}$ [%] | 96.7 | 93.6 | 95.4 | 74.6 | 34.1 | 94.0 |
| $PCC_{NPF}$ [%] | 23.8 | 63.6 | 49.5 | 85.4 | 99.0 | 59.3 |
| $PCC_{tol}$ [%] | 68.5 | 82.0 | 77.8 | 78.8 | 59.2 | 80.6 |
| $\kappa$ | 0.24 | 0.60 | 0.49 | 0.57 | 0.28 | 0.57 |
| PF Region [$10^6$ km$^2$] | 1.63 | – | – | 1.68 | 1.42 | 1.84 |
| PF Area [$10^6$ km$^2$] | – | 1.06 ± 0.09 | 1.13 | 1.00 | 0.76 | 1.25 |
| Reference | Brown (1997) | Zou et al. (2017) | Wu et al. (2018) | Gruber (2012) | Gruber (2012) | Gruber (2012) |

Evaluations are conducted using 1040 aggregated in-situ measurements of permafrost presence or absence. GLM = generalized linear model. PF means permafrost. Norm (normal), warm, and cold means different cases and assumptions of parameters for PZI simulations in $PZI_{global}$ map, details could be found from Table 1 of Gruber (2012). Criteria of continuous means permafrost distribution is compiled as PZI range of [0.01–1]. Some bias is expected for permafrost areas of $QTP_{TIOP}$ and $QTP_{Noah}$ as different QTP boundaries, lake and glacier data are used (Figure 2). Kappa result is interpreted as excellent agreement for $k \geqslant 0.8$, substantial agreement for $0.6 \leqslant k < 0.8$, moderate agreement for 0.4 $\leqslant k < 0.6$, fair agreement for $0.2 \leqslant k < 0.4$, and slight agreement for $k < 0.2$.

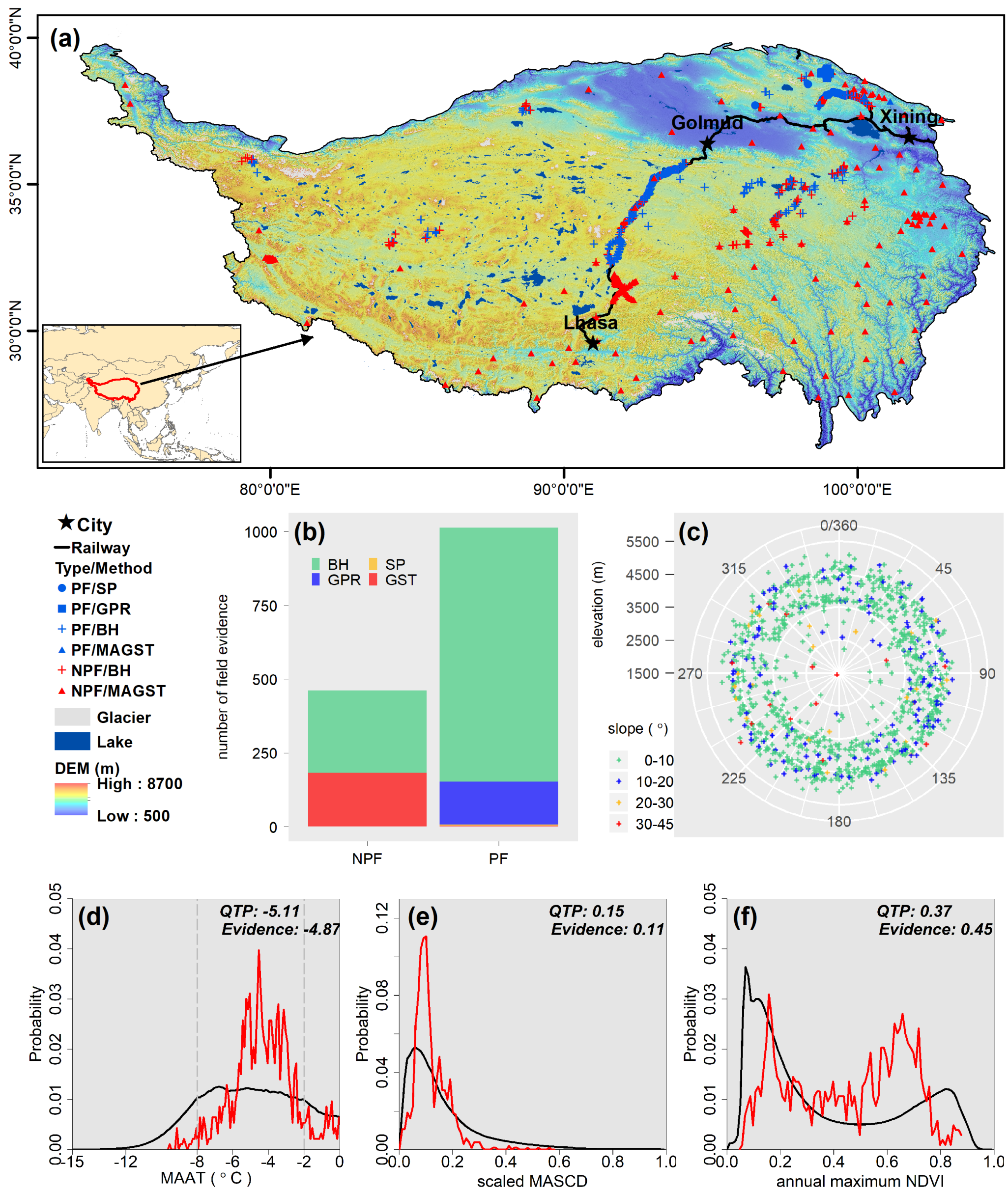


**Figure 1.** (a) The location of the QTP, and in-situ permafrost presence/absence evidence distribution over the QTP, superimposed on the background of digital elevation model (DEM) with 3 arcsec. (c) Number of original field evidence located in permafrost absence (NPF) and presence (PF) regions. BH means field evidence measured by borehole drilling, GPR means ground-penetrating radar, SP means soil pit, and MAGST means mean annual ground surface temperature. (d) Distribution of aggregated field evidence in terms of elevation (radius), slope (colored), and aspect (0/360° represents North). Spread of evidence (red line) for the climate variable of (d) MAAT, (e) scaled MASCD, and (f) annual maximum NDVI comparing to the entire QTP (black line). Numbers in (d), (e), and (f) are mean values. Only the sites/plots with MAAT < 0 °C, which is precondition for permafrost presence, were present in (d).

The Cryosphere Discuss., https://doi.org/10.5194/tc-2018-190
Manuscript under review for journal The Cryosphere
Discussion started: 18 September 2018


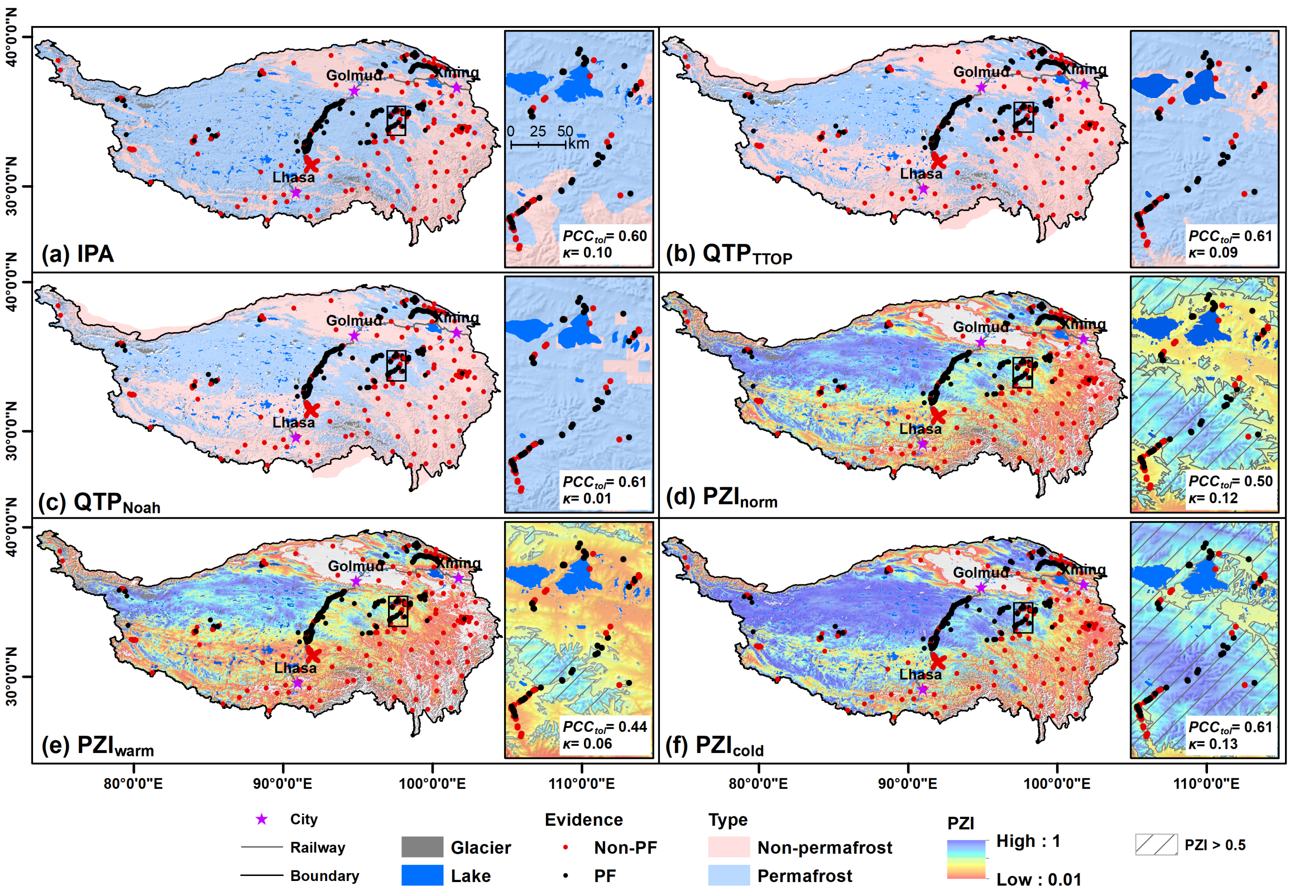


**Figure 2.** The permafrost classification results at in-situ evidence sites/plots in (a) IPA, (b) $\mathrm{QTP_{TTOP}}$, (c) $\mathrm{QTP_{Noah}}$, (d) $\mathrm{PZI_{norm}}$, (e) $\mathrm{PZI_{warm}}$, and (f) $\mathrm{PZI_{cold}}$ maps. $\kappa$ and $PCC$ are the evaluation results for the selected fragile landscapes (marked by black box). All the maps are re-sampled to the unprojected grid of SRTM30 DEM with a resolution of 30 arcsec (∼1 km) to avoid maps bias of with different resolutions, geographic projection, and format. The boundary of QTP used in this study is marked by black line. Binary classification is used for tne $\mathrm{QTP_{TTOP}}$, $\mathrm{QTP_{Noah}}$, and IPA maps, while continuous PZI was present for the $\mathrm{PZI_{norm}}$, $\mathrm{PZI_{warm}}$, $\mathrm{PZI_{cold}}$ maps. The blank part in PZI maps is area with PZI $< 0.01$. The $\kappa$ and $PCC_{\mathrm{tol}}$ present in right small figures were evaluated in the selected areas with 84 evidence.